

Mid-Circuit Cavity Measurement in a Neutral Atom Array

Emma Deist^{1,2,*} Yue-Hui Lu^{1,2,*} Jacquelyn Ho^{1,2} Mary Kate Pasha^{1,2} Johannes Zeiher^{1,3,4}
Zhenjie Yan^{1,2} and Dan M. Stamper-Kurn^{1,2,5,†}


¹*Department of Physics, University of California, Berkeley, California 94720, USA*

²*Challenge Institute for Quantum Computation, University of California, Berkeley, California 94720, USA*

³*Max-Planck-Institut für Quantenoptik, 85748 Garching, Germany*

⁴*Munich Center for Quantum Science and Technology (MCQST), 80799 Munich, Germany*

⁵*Materials Sciences Division, Lawrence Berkeley National Laboratory, Berkeley, California 94720, USA*

 (Received 31 May 2022; revised 19 August 2022; accepted 5 October 2022; published 9 November 2022)

Subsystem readout during a quantum process, or mid-circuit measurement, is crucial for error correction in quantum computation, simulation, and metrology. Ideal mid-circuit measurement should be faster than the decoherence of the system, high-fidelity, and nondestructive to the unmeasured qubits. Here, we use a strongly coupled optical cavity to read out the state of a single tweezer-trapped ^{87}Rb atom within a small tweezer array. Measuring either atomic fluorescence or the transmission of light through the cavity, we detect both the presence and the state of an atom in the tweezer, within only tens of microseconds, with state preparation and measurement infidelities of roughly 0.5% and atom loss probabilities of around 1%. Using a two-tweezer system, we find measurement on one atom within the cavity causes no observable hyperfine-state decoherence on a second atom located tens of microns from the cavity volume. This high-fidelity mid-circuit readout method is a substantial step toward quantum error correction in neutral atom arrays.

DOI: [10.1103/PhysRevLett.129.203602](https://doi.org/10.1103/PhysRevLett.129.203602)

Numerous applications of controlled many-body quantum systems require measurements that read out and affect only a part of the system, i.e., mid-circuit measurements. Examples include quantum error correction [1,2], measurement-based quantum computation [3], quantum-error-corrected metrology [4–6], and an entanglement phase transition induced by mid-circuit measurements on a quantum circuit [7,8]. Effective mid-circuit measurements should satisfy three requirements: they must be faster than the decoherence rate of the system, have low error rates (e.g., below around 1% for implementing surface-code quantum error correction [9–11]), and be sufficiently local so as not to disturb unmeasured quantum bits.

In atom-based systems such as atom-tweezer arrays [12,13], lattice-trapped atoms [14,15], and trapped ion chains [16], the many-atom state is often read out through optical fluorescence imaging. Practical limitations on the numerical aperture (NA) of imaging systems require many photons to be scattered by an atom before it is detected. This requirement impairs the use of free-space imaging for mid-circuit measurement: Measurements tend to be slow (e.g., on the order of 10 [17–21] or 100 ms [22] in atomic tweezer arrays and quantum gas microscopes, respectively [23]), of limited state-detection fidelity owing to spontaneous Raman transitions during detection, and destructive to nearby atoms that can absorb scattered photons.

Here, we demonstrate mid-circuit optical detection of an atomic tweezer array wherein a single atom is measured

with high fidelity while the remaining array retains quantum coherence. For this, we use a strongly coupled cavity to detect a single optical tweezer, allowing for rapid, state-sensitive, high-fidelity, low-atom-loss local measurement with minimal photon scattering of about 100 photons. We benchmark our measurement with a two-atom tweezer array, measuring single atoms sequentially by translating each tweezer trap into the cavity mode, and then detecting light emitted by the cavity that is either fluoresced by the driven atom or transmitted through the driven cavity [Fig. 1(a)]. We observe that an initially prepared hyperfine spin coherence of one atom persists even as the other atom is measured at high fidelity.

Our experimental setup is described in Ref. [26]. Briefly, a bulk optically trapped gas of ultracold ^{87}Rb atoms is prepared near the volume of a horizontal-axis, near-concentric in-vacuum Fabry-Pérot optical cavity with a mirror spacing of 9.4 mm. Atoms are loaded into optical tweezer traps formed by 808-nm-wavelength light that is projected vertically through a high-NA imaging system. An acousto-optical deflector allows us to generate multiple traps in a one-dimensional array and to translate them perpendicularly to the cavity axis. We illuminate the tweezers with counterpropagating light that is detuned about $2\pi \times 35$ MHz below the D_2 $F = 2 \rightarrow F' = 3$ laser-cooling transition, and also with repump light, resonant with the $F = 1 \rightarrow F' = 2$ transition, both at a wavelength of 780 nm. This illumination reduces the population in each tweezer to either zero (empty tweezer) or one atom,

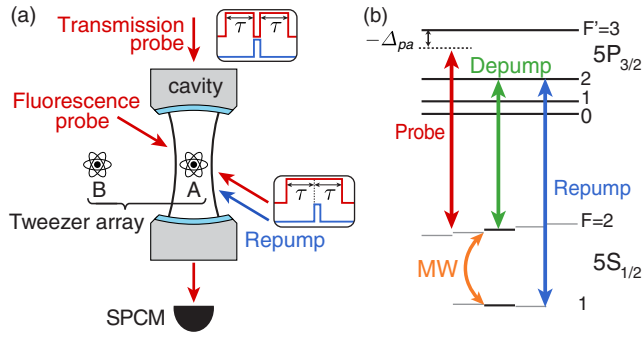


FIG. 1. Experiment schematic. (a) Single atoms are loaded into each of two tweezers that can be translated perpendicularly to the cavity axis for individual readout. Counterpropagating fluorescence probe beams, and also a unidirectional repump beam, are focused on the atom inside the cavity mode. The transmission probe beam couples directly into the cavity. (b) ^{87}Rb level structure. The probe beams (red) are detuned by Δ_{pa} from the $F = 2 \rightarrow F' = 3$ cycling transition. The repump and depump beams (blue and green) are on resonance with the $F = 1 \rightarrow F' = 2$ and $F = 2 \rightarrow F' = 2$ transitions. A resonant microwave (MW) pulse drives the Zeeman-insensitive $|F = 1, m_F = 0\rangle \rightarrow |F = 2, m_F = 0\rangle$ hyperfine transition.

which we distinguish by imaging the resulting fluorescence through the high-NA objective.

Single tweezer-trapped atoms can serve as long-lived qubits by encoding quantum information in the ground-state hyperfine spin [27,28]. Following this approach, we prepare our atoms into the $F = 1$ or $F = 2$ manifold by applying either depump ($F = 2 \rightarrow F' = 2$) or repump light, respectively [29] [Fig. 1(b)]. Combined with information from the aforementioned fluorescence image, the tweezers are thereby prepared in one of three tweezer states: empty, containing an atom in the $F = 1$ manifold, or containing an atom in the $F = 2$ manifold.

We use our cavity to measure a single tweezer, distinguishing each of these three tweezer states. The cavity reaches the single-atom strong coupling regime, with a cooperativity on the ^{87}Rb D_2 cycling transition of $C = g_0^2/(2\kappa\gamma) = 2.3$ with $\{g_0, \kappa, \gamma\} = 2\pi \times \{2.7, 0.53, 3.0\}$ MHz. Here, g_0 is the maximum atom-photon coupling strength between the $F = 2$ and $F' = 3$ stretched states at a field antinode in the center of the TEM_{00} cavity mode with a beam waist of $w_0 = 20(3) \mu\text{m}$. The half-linewidths of the cavity and atomic resonances are κ and γ , respectively.

Our high-cooperativity cavity supports two measurement methods. In the fluorescence method, we directly illuminate the atom and collect its fluorescence using the cavity. Strong atom-cavity coupling results in a large collection efficiency into a single optical mode that is detected with little background noise. In the transmission method, we drive the cavity near its resonance and measure the transmission of cavity probe light. Here, atom-cavity hybridization causes a single atom to broaden (at low C) or split (at high C) the cavity resonance line, reducing the transmitted

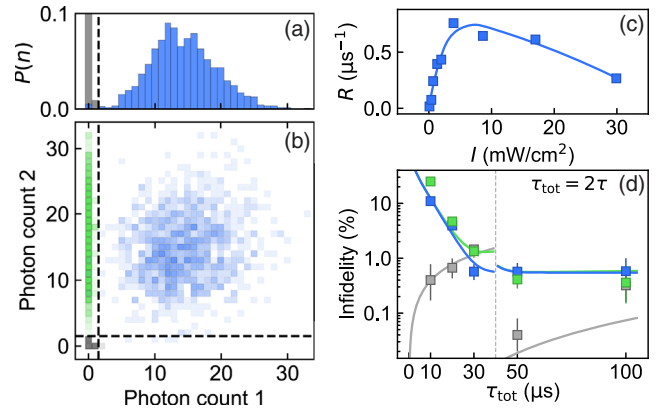


FIG. 2. Fluorescence measurement. A single-probe histogram (a) and two-probe scatter plot (b) show the detected photon counts for tweezers in the no-atom (gray), $F = 2$ atom (blue), or $F = 1$ atom (green) state, taken with $\tau = 25 \mu\text{s}$ and $\Delta_{pc} = -2\pi \times 10$ MHz. The threshold (dashed line) between high and low fluorescence is set between 1 and 2 detected photons. (c) The optimal probe intensity I yields a maximum high count rate of $R = 0.76 \mu\text{s}^{-1}$. Solid line is a guide to the eye. (d) SPAM infidelity is determined for total measurement times $\tau_{\text{tot}} = 2\tau$ from 10 to 100 μs . Solid lines are fits to a model described in Ref. [29]. For $\tau_{\text{tot}} \leq 40 \mu\text{s}$, indicated by the vertical gray line, both the data and model are calculated using a lower detection threshold between 0 and 1 photons.

intensity. Single-atom detection using strongly coupled cavities has been demonstrated previously, through both fluorescence [35,36] and cavity transmission or reflection [35,37]. For a two-atom array, collective detection and one-way transport from a cavity into free space has been demonstrated in Ref. [38], while probabilistic atom-photon conversions with single-atom addressability has been shown in Ref. [39]. The present Letter extends these results to high-fidelity single-atom state detection that does not decohere the rest of the array, demonstrating the necessary features of a mid-circuit measurement in a neutral atom quantum information processor.

In both measurement methods, our goal is to realize three-state sensitivity with measurement infidelity at the subpercent level, as required in certain protocols for quantum error correction [9–11]. We do this by probing the atom-cavity system in two consecutive probe intervals. In each interval of duration τ , using probe light near the $F = 2 \rightarrow F' = 3$ transition, we determine whether the cavity contains a single atom in the $F = 2$ manifold. This is done by counting photons emitted from the cavity using a single-photon counting module (SPCM) with a total quantum efficiency of $\eta = 0.25$ [29]. The detection path and SPCM are polarization-insensitive. A positive detection of an $F = 2$ atom is indicated by the observed photon number being either higher [fluorescence; see Fig. 2(a)] or lower [transmission; see Fig. 3(a)] than an optimized threshold. The second probe interval begins with (for fluorescence) or is preceded by (for transmission) a $\tau_{\text{rp}} = 5 \mu\text{s}$ pulse of localized repump light

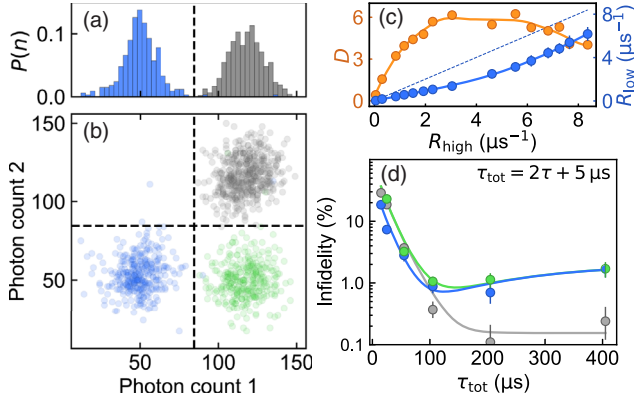


FIG. 3. Transmission measurement. A single-probe histogram (a) and two-probe scatter plot (b) show the detected photon counts for tweezers in the no-atom (gray), $F = 2$ atom (blue), or $F = 1$ atom (green) state, taken with $\tau = 50 \mu\text{s}$ and $\Delta_{pc} = 0$. The threshold (dashed line) between high and low transmission is set above 77 detected photons. (c) The transmitted photon count rate with an $F = 2$ atom in the cavity (R_{low} , blue) is lower than the rate (R_{high} , x axis and dotted line) observed without. Ashman's D (orange), a measure of the separation between R_{low} and R_{high} , reaches a maximum owing to atomic saturation. Lines are guides to the eye. (d) SPAM infidelity is determined for each of the initial tweezer states, with total measurement times $\tau_{\text{tot}} = 2\tau + 5 \mu\text{s}$ ranging from 15 to 205 μs . The threshold between high and low is selected to minimize infidelity at each τ . Lines are fits to a model described in Ref. [29].

[Fig. 1(a) insets]. The negative detection of an $F = 2$ atom in the first interval followed by a positive detection in the second interval measures the tweezer as having contained an $F = 1$ atom, whereas a negative detection in both intervals measures the tweezer as being empty.

In the cavity fluorescence method, we set the cavity resonance frequency ω_c to be detuned by $\Delta_{ca} = \omega_c - \omega_a = -2\pi \times 10 \text{ MHz}$ below the laser-cooling transition frequency ω_a . We illuminate the atom with vertically counterpropagating probe beams in a lin-perp-lin configuration in order to provide polarization gradient cooling during measurements. The probe frequency ω_p is tuned slightly below the cavity resonance ($\Delta_{pc} = \omega_p - \omega_c \sim -\kappa/2$) to realize cavity cooling of the atomic motion [40]. The probe light intensity is set to maximize the photodetection rate $R = R_{\text{max}}$ of an $F = 2$ tweezed atom in

the cavity [Fig. 2(c)]; lower probe intensity drives the atom below saturation, whereas higher probe intensity shifts the incoherent fluorescence spectrum outside the bandwidth of the cavity [41,42]. Experimentally, we find $R_{\text{max}} \simeq 0.76 \mu\text{s}^{-1}$, which is below the theoretical maximum of $R_0 = \eta g_0^2 / (4\kappa) = 5.4 \mu\text{s}^{-1}$ predicted for a two-level atom [29]. This difference may be explained by two effects. First, the tweezer-trapped atom is poorly localized along the cavity axis, exhibiting rms position fluctuations of up to 200 nm with respect to the standing-wave pattern (periodicity of 390 nm) of the cavity mode; see Ref. [26]. The effective square of the atom-cavity coupling strength is thus averaged roughly to $g_{\text{eff}}^2 \simeq g_0^2/2$ owing to spatial random sampling. Second, internal state dynamics induced by the probe light drives the atom between Zeeman sublevels of the ground and excited states, reducing the effective time-averaged coupling to the two polarization modes supported by the cavity. We estimate this effect reduces the maximum cavity emission rate by an additional factor of 0.28 [29].

Fluorescence measurement outcomes, obtained after preparing a single intracavity tweezer in each of the three tweezer states, are shown in Fig. 2. For a probe interval of $\tau = 25 \mu\text{s}$, we observe a large contrast between the photon number detected for a tweezer prepared in the $F = 2$ state and that detected for either the no-atom or $F = 1$ states [Fig. 2(a)]. Combining data from two consecutive 25 μs probe intervals (total measurement time of $\tau_{\text{tot}} = 2\tau = 50 \mu\text{s}$), and setting the threshold for state detection between 1 and 2 photons, we achieve a state preparation and measurement (SPAM) error of several times 10^{-3} for each of the three initial tweezer states (Table I). For shorter τ [Fig. 2(d)], statistical fluctuations in the detected photon number lead us to misidentify bright states as dark states in either the first or second probe intervals, leading to infidelity in $F = 2$ and $F = 1$ state detection, respectively. For longer τ , state preparation error and false detection error caused by the depumping of an $F = 2$ atom before detecting an above-threshold number of photons set a limit on the achievable fidelity. We estimate that these two error sources contribute roughly equally to the overall SPAM error [29]. Table I also reports low atom loss probabilities on the order of 1%, with higher loss rates for atoms in the $F = 2$ manifold due to scattering-induced heating through both probe intervals.

TABLE I. Measurement infidelity and loss probability.

		No atom	$F = 1$	$F = 2$
Fluorescence $2 \times (\tau = 25 \mu\text{s})$	Outcome	Low-low	Low-high	High-X
	Infidelity	0.04(3)%	0.4(2)%	0.6(2)%
	Loss probability		0.2(2)%	1.4(3)%
Transmission $2 \times (\tau = 50 \mu\text{s}) + 5 \mu\text{s}$	Outcome	High-high	High-low	Low-X
	Infidelity	0.4(1)%	1.1(2)%	0.9(2)%
	Loss probability		0.7(3)%	1.4(2)%

In the cavity transmission method, we drive the cavity with light that is resonant with both the cavity and the atom ($\Delta_{ca} = \Delta_{pc} = 0$). The circularly polarized probe light, together with a weak magnetic field applied along the cavity axis, pumps $F = 2$ atoms into the spin-stretched state, maximizing their coupling to the cavity. For weak probe light, we observe that an $F = 2$ atom in the cavity reduces the detected transmitted photon rate R_{low} to 0.4 times the rate R_{high} observed with either no atoms or an $F = 1$ atom in the cavity. For low saturation, one would expect $R_{\text{low}}/R_{\text{high}} = (1 + 2C)^{-2}$ for fixed atom-cavity coupling strength. Averaging this expression over a uniform atomic spatial distribution along the cavity axis yields $R_{\text{low}}/R_{\text{high}} = 0.27$ for our system. The difference between the observed and expected transmission reduction may be explained by an inhomogeneous broadening of the atomic resonance of roughly 4 MHz, caused by the ac Stark shift of the tweezer trap light [35]. At high probe intensity, atomic saturation leads to $R_{\text{high}} - R_{\text{low}}$ reaching a constant difference of roughly $2.4 \mu\text{s}^{-1}$. At an intermediate probe intensity setting of $R_{\text{high}} \simeq 2.2 \mu\text{s}^{-1}$, the bimodal separation statistic D [43] between the high and low photon count distributions reaches its maximum [Fig. 3(c)].

Transmission measurements made at this optimal probe intensity, with two probe intervals of $\tau = 50 \mu\text{s}$ each ($\tau_{\text{tot}} = 2\tau + 5 \mu\text{s} = 105 \mu\text{s}$), again show clear distinctions among tweezers prepared initially in each of the three tweezer states [Fig. 3(a)]. The detection infidelities and atom loss (Table I) are comparable to those obtained through fluorescence. However, the smaller contrast between high and low detection rates causes the transmission method to be generically slower than the fluorescence method of detection. Transmission measurements with a higher C would be interaction-free [45], thus suppressing depumping errors and mechanical effects from light scattering, which provides particular advantages for detecting trapped particles, such as single molecules [46,47], that lack a cycling optical transition.

Next, we demonstrate that our cavity-enhanced detection of one atom does not perturb the quantum evolution of other atoms in an array, an essential requirement for a mid-circuit measurement. We implement a simple quantum circuit consisting of single-qubit gates, realizing a Ramsey sequence on a two-atom tweezer system [Fig. 4(a)]. We form the array with atom A initially trapped within, and atom B at a variable radial distance d outside, the cavity. Both atoms are initialized in the $|F = 2, m_F = 0\rangle$ state and subject to a $\pi/2$ microwave-induced rotation to the $|F = 1, m_F = 0\rangle$ state [29]. A mid-circuit measurement is performed on atom A, using either detection method with the optimal probe times in Table I. We complete the circuit by applying a second $\pi/2$ pulse with a variable phase offset ϕ , translating atom B into and atom A out of the cavity simultaneously within $200 \mu\text{s}$, and performing a cavity measurement of atom B.

Measurements on atom B show a characteristic Ramsey fringe as ϕ is varied [Fig. 4(b)]. We quantify the effect of mid-circuit measurement by considering a normalized contrast, taken as the ratio of the Ramsey-fringe contrasts with and without mid-circuit measurement [48]. We observe a normalized Ramsey contrast above 97% with 84% confidence level [29], when atom B is $d = 34.5 \mu\text{m}$ ($d = 46.0 \mu\text{m}$) away from the cavity mode center for fluorescence (transmission) measurement. A mid-circuit fluorescence measurement begins to affect the coherence of atom B once atom B is within about $20 \mu\text{m}$ of the cavity center [49]. This length scale is consistent with the beam waists of the fluorescence probe beams [29]. A transmission measurement begins to affect atom B at a larger distance of roughly $35 \mu\text{m}$ from the cavity center, consistent with the beam waist of the cavity mode [26].

Our Letter demonstrates that the integration of cavity-enhanced measurement with a configurable tweezer array enables mid-circuit measurement within a neutral atom quantum information platform. We achieve measurement infidelities comparable to the best previous results in

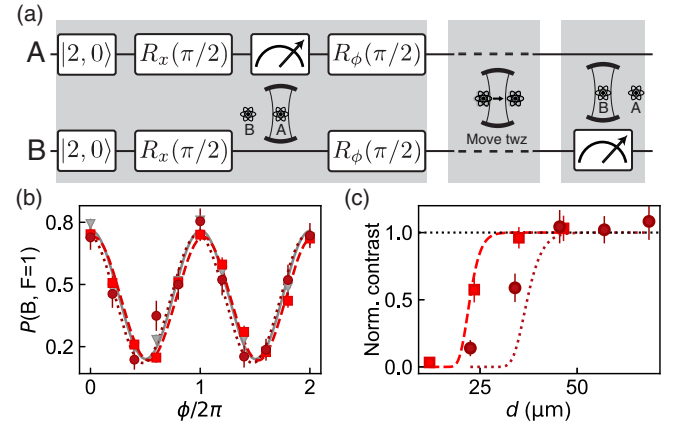


FIG. 4. Mid-circuit measurement. (a) Quantum circuit representing a Ramsey sequence with a mid-circuit measurement of atom A. Atom A (B) is initially located inside (outside) the cavity. Both atoms undergo two $\pi/2$ rotation pulses with variable relative phase ϕ , denoted as $R_x(\pi/2)$ and $R_\phi(\pi/2)$. Atom A is measured between the two pulses using either fluorescence or transmission measurement methods. Both tweezers are repositioned before atom B is measured using the same method. (b) The $F = 1$ state probability of atom B, $P(B, F = 1)$, shows Ramsey fringes as the phase ϕ of the second pulse is varied. We observe no distinction between Ramsey fringes measured following fluorescence (light red squares, $\tau = 25 \mu\text{s}$) and transmission (dark red circles, $\tau = 50 \mu\text{s}$) detections of atom A, and no detection of atom A (gray). Normalized contrast is defined as the ratio of the Ramsey-fringe contrasts observed with and without a mid-circuit measurement on atom A. (c) Normalized contrast versus the initial distance of atom B from the cavity center, with τ settings as in (b). The dashed (dotted) line is a theoretical estimate based on the intensity and size of the fluorescence probe beam (cavity mode) [29].

atomic tweezer systems [20], in a manner that not only allows subsystem-selective measurement but is also fast, with the measurement time being shorter than not only the second-scale hyperfine-state coherence of tweezer-trapped atoms [51,52], but also the $\sim 100 \mu\text{s}$ lifetime of the Rydberg states commonly used in Rydberg-tweezer systems [53]. Combined with the low probability of losing a trapped atom during detection, cavity-based measurement could also enable the deterministic preparation of atom arrays assembled atom by atom, without requiring free-space imaging and resorting [12,13,54–56].

The detection time, infidelity, and loss of our measurement could be reduced further by several experimental improvements. Increasing g_0 and κ simultaneously, up until the onset of hyperfine-state mixing [38], would allow for more efficient and faster detection of scattered photons. Better constraints on atomic motion, achieved by improved laser cooling [29] or by stronger confinement along the cavity axis, would mitigate the effective motional reduction of atom-cavity coupling that we presently observe. Speed limits imposed by the need to transport atoms into the cavity prior to measurement could be improved by employing optical-lattice-based conveyors [57]. Transport could be eliminated altogether by maintaining the tweezer array entirely within the cavity volume and using rapid ac Stark shifts realized with local illumination to bring atoms selectively into resonance with the cavity for detection [21]. The atom loss probability could be reduced by using real-time processing and an adaptive measurement that stops each probe interval when a measurement outcome is obtained [58], and also by applying laser cooling briefly after detection.

We thank C. Liu for assistance in the lab and J. Gerber for comments on the manuscript. We acknowledge support from the AFOSR (Grant No. FA9550-19-10328), from ARO through the MURI program (Grant No. W911NF-20-1-0136), from DARPA (Grant No. W911NF2010090), and from the NSF QLCI program through Grant No. OMA-2016245. E.D. acknowledges support from the NSF Graduate Research Fellowship Program. J.H. acknowledges support from the NIH Molecular Biophysics Training Grant (Grant No. 5T32GM008295-31). J.Z. acknowledges support from the BMBF through the program “Quantum technologies—from basic research to market” (Grant No. 13N16265).

*These authors contributed equally to this work.

[†]dmsk@berkeley.edu

- [1] P. W. Shor, Scheme for reducing decoherence in quantum computer memory, *Phys. Rev. A* **52**, R2493 (1995).
- [2] A. M. Steane, Error Correcting Codes in Quantum Theory, *Phys. Rev. Lett.* **77**, 793 (1996).
- [3] R. Raussendorf and H. J. Briegel, A One-Way Quantum Computer, *Phys. Rev. Lett.* **86**, 5188 (2001).
- [4] E. M. Kessler, I. Lovchinsky, A. O. Sushkov, and M. D. Lukin, Quantum Error Correction for Metrology, *Phys. Rev. Lett.* **112**, 150802 (2014).
- [5] W. Dür, M. Skotiniotis, F. Fröwis, and B. Kraus, Improved Quantum Metrology Using Quantum Error Correction, *Phys. Rev. Lett.* **112**, 080801 (2014).
- [6] S. Zhou and L. Jiang, Optimal approximate quantum error correction for quantum metrology, *Phys. Rev. Res.* **2**, 013235 (2020).
- [7] Y. Li, X. Chen, and M. P. A. Fisher, Quantum Zeno effect and the many-body entanglement transition, *Phys. Rev. B* **98**, 205136 (2018).
- [8] B. Skinner, J. Ruhman, and A. Nahum, Measurement-Induced Phase Transitions in the Dynamics of Entanglement, *Phys. Rev. X* **9**, 031009 (2019).
- [9] E. Dennis, A. Kitaev, A. Landahl, and J. Preskill, Topological quantum memory, *J. Math. Phys. (N.Y.)* **43**, 4452 (2002).
- [10] R. Raussendorf and J. Harrington, Fault-Tolerant Quantum Computation with High Threshold in Two Dimensions, *Phys. Rev. Lett.* **98**, 190504 (2007).
- [11] A. G. Fowler, M. Mariantoni, J. M. Martinis, and A. N. Cleland, Surface codes: Towards practical large-scale quantum computation, *Phys. Rev. A* **86**, 032324 (2012).
- [12] D. Barredo, S. D. Léseleuc, V. Lienhard, T. Lahaye, and A. Browaeys, An atom-by-atom assembler of defect-free arbitrary two-dimensional atomic arrays, *Science* **354**, 1021 (2016).
- [13] M. Endres, H. Bernien, A. Keesling, H. Levine, E. R. Anschuetz, A. Krajenbrink, C. Senko, V. Vuletić, M. Greiner, and M. D. Lukin, Atom-by-atom assembly of defect-free one-dimensional cold atom arrays, *Science* **354**, 1024 (2016).
- [14] Y. Wang, X. Zhang, T. A. Corcovilos, A. Kumar, and D. S. Weiss, Coherent Addressing of Individual Neutral Atoms in a 3D Optical Lattice, *Phys. Rev. Lett.* **115**, 043003 (2015).
- [15] C. Gross and I. Bloch, Quantum simulations with ultracold atoms in optical lattices, *Science* **357**, 995 (2017).
- [16] C. D. Bruzewicz, J. Chiaverini, R. McConnell, and J. M. Sage, Trapped-ion quantum computing: Progress and challenges, *Appl. Phys. Rev.* **6**, 021314 (2019).
- [17] A. Fuhrmanek, R. Bourgain, Y. R. P. Sortais, and A. Browaeys, Free-Space Lossless State Detection of a Single Trapped Atom, *Phys. Rev. Lett.* **106**, 133003 (2011).
- [18] M. Kwon, M. F. Ebert, T. G. Walker, and M. Saffman, Parallel Low-Loss Measurement of Multiple Atomic Qubits, *Phys. Rev. Lett.* **119**, 180504 (2017).
- [19] M. Martinez-Dorantes, W. Alt, J. Gallego, S. Ghosh, L. Ratschbacher, Y. Völzke, and D. Meschede, Fast Nondestructive Parallel Readout of Neutral Atom Registers in Optical Potentials, *Phys. Rev. Lett.* **119**, 180503 (2017).
- [20] J. P. Covey, I. S. Madjarov, A. Cooper, and M. Endres, 2000-Times Repeated Imaging of Strontium Atoms in Clock-Magic Tweezer Arrays, *Phys. Rev. Lett.* **122**, 173201 (2019).
- [21] A. Urech, I. H. A. Knottnerus, R. J. C. Spreeuw, and F. Schreck, Narrow-line imaging of single strontium atoms in shallow optical tweezers, *Phys. Rev. Res.* **4**, 023245 (2022).

- [22] C. Gross and W.S. Bakr, Quantum gas microscopy for single atom and spin detection, *Nat. Phys.* **17**, 1316 (2021).
- [23] We note recent efforts that achieve fast free-space detection of tweezer-trapped neutral atoms through careful engineering of fluorescence detection [24] and Rydberg-ensemble-assisted imaging [25].
- [24] A. Bergschneider, V.M. Klinkhamer, J.H. Becher, R. Klemt, G. Zürn, P.M. Preiss, and S. Jochim, Spin-resolved single-atom imaging of ^6Li in free space, *Phys. Rev. A* **97**, 063613 (2018).
- [25] W. Xu, A.V. Venkatramani, S.H. Cantú, T. Šumarac, V. Klüsener, M.D. Lukin, and V. Vuletić, Fast Preparation and Detection of a Rydberg Qubit Using Atomic Ensembles, *Phys. Rev. Lett.* **127**, 050501 (2021).
- [26] E. Deist, J.A. Gerber, Y.-H. Lu, J. Zeiher, and D.M. Stamper-Kurn, Superresolution Microscopy of Optical Fields Using Tweezer-Trapped Single Atoms, *Phys. Rev. Lett.* **128**, 083201 (2022).
- [27] T. Xia, M. Lichtman, K. Maller, A.W. Carr, M.J. Piotrowicz, L. Isenhower, and M. Saffman, Randomized Benchmarking of Single-Qubit Gates in a 2D Array of Neutral-Atom Qubits, *Phys. Rev. Lett.* **114**, 100503 (2015).
- [28] H. Levine, A. Keesling, G. Semeghini, A. Omran, T.T. Wang, S. Ebadi, H. Bernien, M. Greiner, V. Vuletić, H. Pichler, and M.D. Lukin, Parallel Implementation of High-Fidelity Multiqubit Gates with Neutral Atoms, *Phys. Rev. Lett.* **123**, 170503 (2019).
- [29] See Supplemental Material at <http://link.aps.org/supplemental/10.1103/PhysRevLett.129.203602> for details on experimental methods and data analysis, which includes Refs. [30–34].
- [30] N. Schlosser, G. Reymond, I. Protsenko, and P. Grangier, Sub-poissonian loading of single atoms in a microscopic dipole trap, *Nature (London)* **411**, 1024 (2001).
- [31] C. Tuchendler, A.M. Lance, A. Browaeys, Y.R.P. Sortais, and P. Grangier, Energy distribution and cooling of a single atom in an optical tweezer, *Phys. Rev. A* **78**, 033425 (2008).
- [32] A.M. Kaufman, B.J. Lester, and C.A. Regal, Cooling a Single Atom in an Optical Tweezer to Its Quantum Ground State, *Phys. Rev. X* **2**, 041014 (2012).
- [33] J.A. Gerber, Cavity quantum electrodynamics with a locally addressable quantum gas, Ph.D. thesis, University of California Berkeley, 2020.
- [34] J.R. Johansson, P.D. Nation, and F. Nori, QuTiP2: A PYTHON framework for the dynamics of open quantum systems, *Comput. Phys. Commun.* **184**, 1234 (2013).
- [35] J. Bochmann, M. Mücke, C. Guhl, S. Ritter, G. Rempe, and D.L. Moehring, Lossless State Detection of Single Neutral Atoms, *Phys. Rev. Lett.* **104**, 203601 (2010).
- [36] J. Gallego, W. Alt, T. Macha, M. Martinez-Dorantes, D. Pandey, and D. Meschede, Strong Purcell Effect on a Neutral Atom Trapped in an Open Fiber Cavity, *Phys. Rev. Lett.* **121**, 173603 (2018).
- [37] R. Gehr, J. Volz, G. Dubois, T. Steinmetz, Y. Colombe, B. L. Lev, R. Long, J. Estève, and J. Reichel, Cavity-Based Single Atom Preparation and High-Fidelity Hyperfine State Readout, *Phys. Rev. Lett.* **104**, 203602 (2010).
- [38] T. Dordevic, P. Samutpraphoot, P.L. Ocola, H. Bernien, B. Grinkemeyer, I. Dimitrova, V. Vuletić, and M.D. Lukin, Entanglement transport and a nanophotonic interface for atoms in optical tweezers, *Science* **373**, 1511 (2021).
- [39] S. Langenfeld, O. Morin, M. Körber, and G. Rempe, A network-ready random-access qubits memory, *npj Quantum Inf.* **6**, 86 (2020).
- [40] S. Nuszmann, K. Murr, M. Hijkema, B. Weber, A. Kuhn, and G. Rempe, Vacuum-stimulated cooling of single atoms in three dimensions, *Nat. Phys.* **1**, 122 (2005).
- [41] B.R. Mollow, Power spectrum of light scattered by two-level systems, *Phys. Rev.* **188**, 1969 (1969).
- [42] H.J. Kimble and L. Mandel, Theory of resonance fluorescence, *Phys. Rev. A* **13**, 2123 (1976).
- [43] Given two distributions with means $\mu_{1,2}$ and standard deviations $\sigma_{1,2}$, Ashman's D statistic for bimodal separation is defined as $D = |\mu_1 - \mu_2| / \sqrt{(\sigma_1^2 + \sigma_2^2)/2}$; see Ref. [44].
- [44] K.A. Ashman, C.M. Bird, and S.E. Zepf, Detecting bimodality in astronomical datasets, *Astron. J.* **108**, 2348 (1994).
- [45] P. Kwiat, H. Weinfurter, T. Herzog, A. Zeilinger, and M.A. Kasevich, Interaction-Free Measurement, *Phys. Rev. Lett.* **74**, 4763 (1995).
- [46] L. Anderegg, L.W. Cheuk, Y. Bao, S. Burchesky, W. Ketterle, K.-K. Ni, and J.M. Doyle, An optical tweezer array of ultracold molecules, *Science* **365**, 1156 (2019).
- [47] J.T. Zhang, L.R.B. Picard, W.B. Cairncross, K. Wang, Y. Yu, F. Fang, and K.-K. Ni, An optical tweezer array of ground-state polar molecules, *Quantum Sci. Technol.* **7**, 035006 (2022).
- [48] The limited fringe contrast of about 0.6 observed in our setup even without mid-circuit detection arises from imperfect preparation in the $m_F = 0$ magnetic sublevel and ac Stark shifts of the microwave frequency by tweezer light.
- [49] Reference [50] demonstrates fast local detection in a trapped ion platform, with low measurement-induced decoherence for ions with separations of hundreds of micrometers.
- [50] S. Crain, C. Cahall, G. Vrijsen, E.E. Wollman, M.D. Shaw, V.B. Verma, S.W. Nam, and J. Kim, High-speed low-crosstalk detection of a 171Yb^+ qubit using superconducting nanowire single photon detectors, *Commun. Phys.* **2**, 97 (2019).
- [51] D. Bluvstein, H. Levine, G. Semeghini, T.T. Wang, S. Ebadi, M. Kalinowski, A. Keesling, N. Maskara, H. Pichler, M. Greiner, V. Vuletić, and M.D. Lukin, A quantum processor based on coherent transport of entangled atom arrays, *Nature (London)* **604**, 451 (2022).
- [52] M.A. Norcia, A.W. Young, W.J. Eckner, E. Oelker, J. Ye, and A.M. Kaufman, Seconds-scale coherence on an optical clock transition in a tweezer array, *Science* **366**, 93 (2019).
- [53] I.I. Beterov, I.I. Ryabtsev, D.B. Tretyakov, and V.M. Entin, Quasiclassical calculations of blackbody-radiation-induced depopulation rates and effective lifetimes of Rydberg nS , nP , and nD alkali-metal atoms with $n \leq 80$, *Phys. Rev. A* **79**, 052504 (2009).
- [54] Y. Miroshnychenko, W. Alt, I. Dotsenko, L. Förster, M. Khudaverdyan, D. Meschede, D. Schrader, and A. Rauschenbeutel, An atom-sorting machine, *Nature (London)* **442**, 151 (2006).
- [55] K.M. Fortier, S.Y. Kim, M.J. Gibbons, P. Ahmadi, and M.S. Chapman, Deterministic Loading of Individual Atoms

- to a High-Finesse Optical Cavity, *Phys. Rev. Lett.* **98**, 233601 (2007).
- [56] H. Kim, W. Lee, H.-g. Lee, H. Jo, Y. Song, and J. Ahn, *In situ* single-atom array synthesis using dynamic holographic optical tweezers, *Nat. Commun.* **7**, 13317 (2016).
- [57] S. Kuhr, W. Alt, D. Schrader, M. Müller, V. Gomer, and D. Meschede, Deterministic delivery of a single atom, *Science* **293**, 278 (2001).
- [58] M. N. H. Chow, B. J. Little, and Y.-Y. Jau, High-fidelity, low-loss state detection of alkali-metal atoms in optical tweezer traps, *arXiv:2206.00144*.